Aspects of Discontinuous Galerkin Methods for Hyperbolic Conservation Laws

Joseph E. Flaherty Lilia Krivodonova Jean-Francois Remacle
Mark S. Shephard
Scientific Computation Research Center
Rensselaer Polytechnic Institute
Troy, NY 12180-3590

Dedicated in memory of Robert J. Melosh, R.P.I.'47

Abstract

We review several properties of the discontinuous Galerkin method for solving hyperbolic systems of conservation laws including basis construction, flux evaluation, solution limiting, adaptivity, and *a posteriori* error estimation. Regarding error estimation, we show that the leading term of the spatial discretization error using the discontinuous Galerkin method with degree p piecewise polynomials is proportional to a linear combination of orthogonal polynomials on each element of degrees p and $p+1$. These are Radau polynomials in one dimension. The discretization errors have a stronger superconvergence of order $O(h^{2p+1})$, where h is a mesh-spacing parameter, at the outflow boundary of each element. These results are used to construct asymptotically correct *a posteriori* estimates of spatial discretization errors in regions where solutions are smooth.

We present the results of applying the discontinuous Galerkin method to unsteady, two-dimensional, compressible, inviscid flow problems. These include adaptive computations of Mach reflection and mixing-instability problems.

1 Introduction

The discontinuous Galerkin method (DGM) provides an appealing approach to address problems having discontinuities, such as those that arise in hyperbolic conservation laws. Originally developed for neutron transport problems [37] and first analyzed by Le Saint and Raviart [41], the technique lay dormant for approximately fifteen years before becoming popular. It is now being used to solve ordinary differential equations [31] and hyperbolic [10, 11, 12, 13, 18, 17, 20, 23], parabolic [21, 22], and elliptic [9, 8, 48] partial differential equations. A more thorough sampling of the theoretical and applied aspects of the method appears in the proceedings of Cockburn *et al.* [16].

The DGM may be regarded as cross between a finite volume and finite element method and it has many of the good properties of both. Thus, for example:

- The solution space is a piecewise-continuous (polynomial) function relative to a structured or unstructured mesh. As such, it can sharply capture solution discontinuities relative to the computational mesh.
- The DGM simplifies adaptivity since interelement continuity is neither required for h-refinement (mesh refinement and coarsening) nor p-refinement (method order variation).
- The method conserves the appropriate physical quantities (*e.g.*, mass, momentum, and energy) on an elemental basis.
- The method can handle problems in complex geometries to high order.
- Some interesting and useful *a posteriori* error estimates are available [3, 14, 15, 42, 43, 44] for use with adaptivity.
- Regardless of order, the DGM has a simple communication pattern to elements with a common face that simplifies parallel computation [23, 24].

With a discontinuous basis, the DGM produces more unknowns for a given order of accuracy than traditional finite element or finite volume methods and this may lead to some inefficiency. This could be overcome on a parallel computer because of the simpler communication pattern. Reducing the spurious oscillations that arise when high-order methods are applied to problems with discontinuities is a difficulty for all methods for conservation laws. With the DGM, the strategy for controlling oscillations is to limit the variations in the solution and/or flux [13, 17, 18, 45]. While limiting oscillations is relatively well known for finite difference technologies on structured meshes [45], it is still unresolved for DGMs, particularly on unstructured meshes.

Herein, we survey some theoretical and computational aspects of the DGM as it applies to hyperbolic conservation laws of the form

$$\partial_t \mathbf{u} + \mathbf{div}\vec{\mathbf{F}}(\mathbf{u}) = \mathbf{r}(\mathbf{u}). \tag{1a}$$

Variables with a superimposed arrow refer to physical vectors and those in bold type refer to a continuous field (in $(\mathcal{H}^1)^m$). The flux matrix is

$$\vec{\mathbf{F}}(\mathbf{u}) := [\vec{F}_1(\mathbf{u}), \vec{F}_2(\mathbf{u}), \ldots, \vec{F}_m(\mathbf{u})], \tag{1b}$$

where $\vec{F}_i(\mathbf{u})$ is the i^{th} component of the flux $\vec{\mathbf{F}}$, and

$$\mathbf{div} := [\mathrm{div}, \mathrm{div} \ldots, \mathrm{div}]^T \tag{1c}$$

is the vector valued divergence operator.

The system of interest in this work is the two-dimensional Euler equations of compressible, inviscid fluid dynamics where

$$\mathbf{u} = [\rho, \rho v_x, \rho v_y, E]^T, \tag{2a}$$

$$\vec{\mathbf{F}}(\mathbf{u}) = [\rho\vec{v},\ \rho v_x\vec{v} + P\vec{i}_x,\ \rho v_y\vec{v} + P\vec{i}_y,\ (E+P)\vec{v}], \tag{2b}$$

$$\mathbf{r} = \mathbf{0}. \tag{2c}$$

Here, ρ is the density, $\vec{v} = (v_x, v_y)$ is the velocity, E is the internal energy, and P is the pressure of the fluid. The quantities $\vec{i}_x$ and $\vec{i}_y$ are unit vectors in the Cartesian x and y directions, respectively. An equation of state of the form $P = P(\rho, E)$ is necessary to close the system, and we assume the fluid behaves as a perfect gas where

$$P = (\gamma - 1)\rho \left[E - \frac{\|\vec{v}\|^2}{2} \right] \tag{2d}$$

with gas constant $\gamma = 1.4$.

We develop the DGM for (1) using a local formulation of Cockburn *et al.* [17, 18] (§2) and describe some choices for an orthogonal basis (§2.1), numerical flux functions (§2.2), and solution limiting (§2.3). We follow with a description of *a posteriori* error estimation procedures for spatial discretization errors in regions where the solution is smooth (§3). Both one- and multi-dimensional error estimates are based on the existence of a strong superconvergence phenomena at the downwind (outflow) ends of elements. We describe some simple adaptive h- and p-refinement procedures (§4) and use them to address compressible flow problems involving a double Mach reflection from a wedge [19, 49] and a Rayleigh-Taylor flow instability involving the perturbation of a heavy fluid overlying a lighter one (§4.4). These classical problems are used as difficult computational tests for any proposed numerical method intended for compressible flow applications.

2 Discontinuous Galerkin Formulation

As customary with finite element formulations we divide the problem domain Ω into a collection of elements

$$\Omega = \bigcup_{j=1}^{N_h} \Omega_j \tag{3}$$

and assume, for simplicity, that this may be done without error. Following the formulation of Cockburn *et al.* [17, 18], we construct a Galerkin problem on one element Ω_j by multiplying (1) by a test function $\mathbf{v} \in (\mathcal{L}^2(\Omega_j))^m$, integrating the result on Ω_j, and using the divergence theorem to obtain

$$(\mathbf{v}, \partial_t \mathbf{u})_{\Omega_j} - (\mathbf{grad}\mathbf{v}, \vec{\mathbf{F}}(\mathbf{u}))_{\Omega_j} + < \mathbf{v}, \vec{\mathbf{F}}_n >_{\partial\Omega_j} = (\mathbf{v}, \mathbf{r})_{\Omega_j}, \qquad \forall \mathbf{v} \in (\mathcal{L}^2(\Omega_j))^m. \tag{4a}$$

The $\mathcal{L}^2$ volume and surface inner products are

$$(\mathbf{v}, \mathbf{u})_{\Omega_j} = \int_{\Omega_j} \mathbf{v}^T \mathbf{u} d\tau, \qquad < \mathbf{v}, \mathbf{u} >_{\partial\Omega_j} = \int_{\partial\Omega_j} \mathbf{v}^T \mathbf{u} d\sigma. \tag{4b}$$

Several issues must be resolved before the formulation (4) can be used as a numerical method.

- The solution $\mathbf{u}$ must be approximated by functions in a finite-dimensional subspace of the solution space. This is greatly simplified without the need to maintain inter-element continuity. Meshes and approximate solutions such as those shown in

Figure 1 are possible. We select the approximation $\mathbf{U}$ of $\mathbf{u}$ to be a piecewise-polynomial function of degree p relative to the mesh. The basis is chosen to be orthogonal in $\mathcal{L}^2(\Omega_j)$ (*cf.* §2.1 and Remacle *et al.* [38]), which will produce a diagonal mass matrix.

- With a discontinuous basis, the normal flux $\mathbf{F}_n = \vec{\mathbf{F}}(\mathbf{u}) \cdot \vec{n}$, where $\vec{n}$ is the normal vector to $\partial\Omega_j$, is not defined on $\partial\Omega_j$. The usual strategy is to define it in terms of a numerical flux $\mathbf{F}_n(\mathbf{U}_j, \mathbf{U}_k)$ that depends on the solution $\mathbf{U}_j$ on Ω_j and $\mathbf{U}_k$ on the neigboring element Ω_k sharing the portion of the bounday $\partial\Omega_{jk}$ common to both elements (§2.2). The numerical flux is required to be consistent in the sense that $\mathbf{F}_n(\mathbf{u}, \mathbf{u}) = \vec{\mathbf{F}}(\mathbf{u}) \cdot \vec{n}$.

- As previously noted, DGM solutions with $p > 0$ will exhibit spurious oscillations near discontinuities. Techniques to limit solution variation are not generally available. Herein, we use a moment limiting strategy of Biswas *et al.* that has worked well on structured meshes (§2.3).

- With the trial and test spaces being polynomials of degree p on Ω_j, inner products appearing in (4) are done by Gaussian quadrature of order $2p$.

- Time integration is performed by explicit total variation bounded Runge-Kutta integration scheme [18, 5]. Because we are dealing with highly localized phenomena in time and space, we use a local time stepping procedure similar to one used by Flaherty *et al.* [23], which will be described in a forthcoming paper [39].

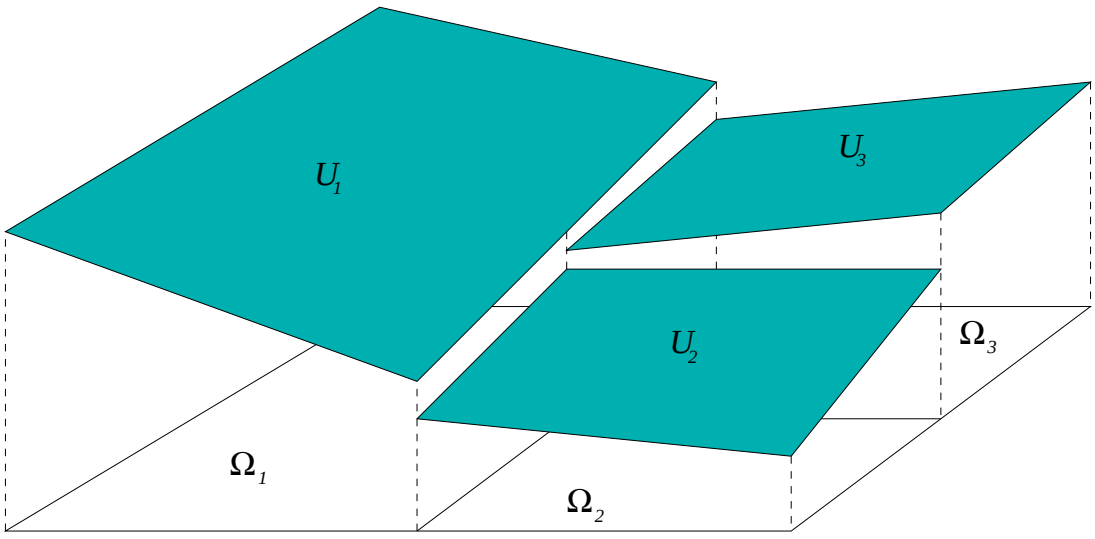

Figure 1: Sample mesh and solution for use with the discontinuous Galerkin method.

2.1 Orthogonal Basis

On each element $\Omega_j \in \Omega$, we approximate $\mathbf{u}$ by a polynomial $\mathbf{U} \in (\mathcal{P}^{p_j})^m \subset (\mathcal{H}^1(\Omega_j))^m$, where $\mathcal{P}^{p_j}$ is a space of polynomials of degree p_j on Ω_j. (When not emphasizing the

variation of degree p_j, we will suppress the subscript j.) Since the approximation is only continuous on elements, the global approximation on Ω may have jump discontinuities at element boundaries. Without the need to maintain interelement continuity, the choice of basis for $\mathcal{P}^p$ is essentially unrestricted. Nevertheless, some basis choices will be more convenient and computationally efficient than others. We construct an orthogonal basis for $\mathcal{P}^p$ relative to the $\mathcal{L}^2(\Omega_j)$ inner product. As a result, the mass matrix will be diagonal and time integration will neither necessitate "lumping" nor matrix inversion. The orthogonal basis also simplifies adaptive p-refinement.

Orthogonal bases on quadrilateral elements may be constructed as tensor products of Legendre polynomials. Basis construction on triangles proceeds by mapping Ω_j in the (x, y)-plane onto the usual canonical, unit, right-triangular element $\{(\xi, \eta) | 0 \leq \xi, \eta \leq 1,\ \xi + \eta \leq 1\}$.

To begin, consider a basis for $\mathcal{P}^p$ in terms of monomials in (ξ, η), *i.e.*,

$$B = \{b_i, i = 1, 2, \ldots, N_p\} = \{1, \xi, \eta, \xi^2, \xi\eta, \eta^2, \ldots, \eta^p\}, \tag{5}$$

with $N_p = (p + 1)(p + 2)/2$. We seek an alternate basis $G = \{g_i, i = 1, 2, \ldots, N_p\}$ of $\mathcal{P}^p$ which is orthonormal in $\mathcal{L}^2(\Omega_0)$; thus, $(g_i, g_k)_{\Omega_j} = \delta_{ik}$, $i, k = 1, 2, \ldots, N_p$. This may be done by applying Gram-Schmidt orthonormalization [27] to the basis B. Thus, we compute

$$g_i = \frac{b_i - \sum_{k=1}^{i-1}(b_i, g_k)g_k}{\sqrt{(b_i, b_i - \sum_{k=1}^{i-1}(b_i, g_k)g_k)}} \qquad i = 1, 2, \ldots, N_p. \tag{6}$$

with the understanding that summations are zero when their upper limit is less than their lower one. Since b_k has the form $b_k = \xi^{\alpha(k)}\eta^{\beta(k)}$ with exponents $\alpha(k)$ and $\beta(k)$ depending on k, inner products may be calculated as [38]

$$(b_i, b_k)_{\Omega_0} = \int_0^1 \int_0^{1-\xi} \xi^m \eta^n \, d\xi d\eta = \frac{1}{n+1} \sum_{l=0}^{n+1} \frac{C_n^l}{m + l + 1} \tag{7}$$

with $m = \alpha(i) + \alpha(k)$ and $n = \beta(i) + \beta(k)$. The result (7) avoids numerical integration in the Gram-Schmidt process, so that shape functions can be computed to any order without a loss of precision.

The $\mathcal{L}^2(\Omega_j)$ orthogonality of g_i, $i = 1, 2, \ldots, N_p$, will only be preserved in the physical (x, y) space if the mapping from the physical to the computational space is linear, *i.e.*, the Jacobian of the mapping is constant. Curved elements, which are essential for higher-order analysis on curved domains [8], will require some modifications. For example Gram-Schmidt orthogonalization can be performed relative to a Jacobian-weighted inner product and induced norm. Shape functions would become element dependent and the orthogonalization would have to be computed and stored for every curved element of the mesh. This is not excessive because the total memory never exceeds that required for a global mass matrix and the number of curved elements is typically $O(\sqrt{N_h})$ for a problem with N_h elements.

2.2 Numerical Flux

Upon choosing a numerical normal flux $\mathbf{F}_n(\mathbf{U}_j, \mathbf{U}_k)$ on the face $\partial\Omega_{jk}$ separating elements j and k, the DGM (4a) becomes

$$(\mathbf{V}, \partial_t \mathbf{U})_{\Omega_j} - (\mathbf{grad}\mathbf{V}, \vec{\mathbf{F}}(\mathbf{U}))_{\Omega_j} \quad + \quad \sum_{k=1}^{n_{\partial\Omega_j}} < \mathbf{V}, \mathbf{F}_n(\mathbf{U}_j, \mathbf{U}_k) >_{\partial\Omega_j} = (\mathbf{V}, \mathbf{r})_{\Omega_j}, \quad \forall \mathbf{V} \in (\mathcal{P}^p(\Omega_j))^m, \tag{8}$$

where $n_{\partial\Omega_j}$ is the number of faces of Ω_j.

A common strategy [5, 17, 18] is to compute the numerical normal flux as the exact or approximate flux of a Riemann problem breaking on $\partial\Omega_{jk}$. Recall that a Riemann problem is an initial value (Cauchy) problem with piecewise constant data. Several choices are possible [18, 40, 35, 49]. Regardless of whether the problem is one-, two-, or three-dimensional, only the normal component of the numerical flux need be defined and this greatly simplifies the task. The most direct choice is the *upwind* flux where the numerical flux is computed using $\mathbf{F}_n(\mathbf{U}_k)$ on $\partial\Omega_{jk}$ if the flow is into Ω_j and $\mathbf{F}_n(\mathbf{U}_j)$ in the opposite case. The *Lax-Freidrichs* flux

$$\mathbf{F}_n(\mathbf{U}_j, \mathbf{U}_k) = \frac{1}{2}[\mathbf{F}_n(\mathbf{U}_j) + \mathbf{F}_n(\mathbf{U}_k) - \lambda_{max}(\mathbf{U}_j - \mathbf{U}_k)] \tag{9}$$

is only slightly more complex. Here, λ_{max} is the maximum absolute eigenvalue of the Jacobian $\partial\mathbf{F}_n(\mathbf{u})/\partial\mathbf{u}$ using, *e.g.*, $\mathbf{u} = (\mathbf{U}_j + \mathbf{U}_k)/2$. Roe [40] computed the numerical flux as the exact flux of a linearized Riemann problem across the interface. This required some care to ensure that entropy conditions were not violated [28]. Van Leer [35] split the normal flux into components having Jacobians with only positive and negative eigenvalues. With this, he constructed numerical fluxes that were continuously differentiable across a shock discontinuity. Woodward and Colella [49]constructed a numerical flux that reduced excessive diffusion near contact discontinuities. Other flux choices appear in Cockburn and Shu [18].

2.3 Limiting

The goal of a limiting strategy is to reduce or eliminate the spurious oscillations that develop near discontinuities with high-order ($p > 0$) methods without reducing accuracy in regions where solutions are smooth. In their original work, Cockburn and Shu [18] used a strategy to limit the variation of solution slopes. For simplicity, we will present this for a one-dimensional scalar problem. The Legendre polynomials are orthogonal in this case, and solutions on $\Omega_j := \{x | x_{j-1}, x_j\}$ are approximated as

$$U_j(x,t) = \sum_{k=0}^{p} c_{jk}(t) P_k(\xi(x)) \tag{10a}$$

where

$$\xi(x) = \frac{2x - (x_j + x_{j-1})}{x_j - x_{j-1}} \tag{10b}$$

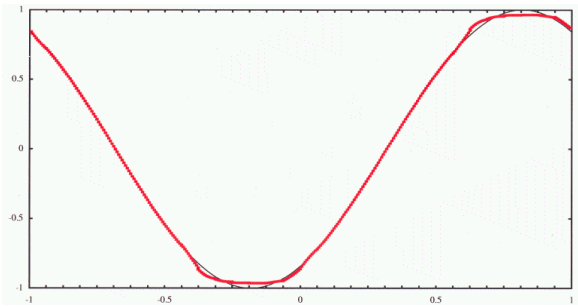

Figure 2: DGM solution of Example 1 at $t = 1$ with $p = 2$ and $N_h = 32$ using slope limiting [13]. The exact solution is shown in black and the computed solution in red.

and $P_k(\xi)$ is the Legendre polynomial of degree k in $\xi \in [-1, 1]$.

With a slope limiting procedure [18], one calculates modified deviations at the ends x_{j-1} and x_j of Ω_j as

$$S_{1,j} = \text{minmod}(U_j(x_j, t) - \bar{U}_j, \Delta\bar{U}_j, \nabla\bar{U}_j), \tag{11a}$$

$$S_{-1,j} = \text{minmod}(\bar{U}_j - U_j(x_{j-1}, t), \Delta\bar{U}_j, \nabla\bar{U}_j) \tag{11b}$$

where $\bar{U}_j$ is the solution average on Ω_j,

$$\text{minmod}(a, b, c) = \begin{cases} \min(a, b, c), & \text{if } \text{sgn}(a) = \text{sgn}(b) = \text{sgn}(c) \\ 0, & \text{otherwise} \end{cases}, \tag{11c}$$

$$\Delta\bar{U}_j := U_{j+1} - U_j, \qquad \nabla\bar{U}_j := U_j - U_{j-1} \tag{11d}$$

These modified deviations are used to calculate modified solution coefficients in (10a) as

$$S_{1,j} = U_j(x_j, t) - \bar{U}_j, \qquad S_{-1,j} = \bar{U}_j - U_j(x_{j-1}, t). \tag{11e}$$

Since these represent two equations for p unknowns, unique solutions do not exist when $p > 2$. One possibility [18] is to set $c_k = 0$, $k = 3, 4, \ldots, p$. This, however, may reduce the order of accuracy should the limiting procedure modify the solution in a region not containing discontinuities.

Example 1. We solve the initial value problem for the kinematic wave equation

$$u_t + u_x = 0, \qquad t > 0, \qquad u(x, 0) = \sin \pi x \tag{12}$$

on a periodicity cell $-1 \le x < 1$ using the DGM with $p = 2$ and $N_h = 32$. Although limiting is not necessary since solutions are smooth, we apply slope limiting (11) to obtain the solution shown in Figure 2 at $t = 1$. The solution has been "flattened" near the smooth extrema and the convergence rate has been reduced [13].

Biswas *et al.* [13] tried to overcome the loss of accuracy in smooth solution regions by applying the slope limiting procedure (11) in an adaptive manner to successively lower-order coefficients in (10a). In particular, they limited $c_{k+1,j}$ as

$$(2k + 1)c_{k+1,j} = \text{minmod}((2k + 1)c_{k+1,j}, \Delta c_{kj}, \nabla c_{kj}). \tag{13}$$

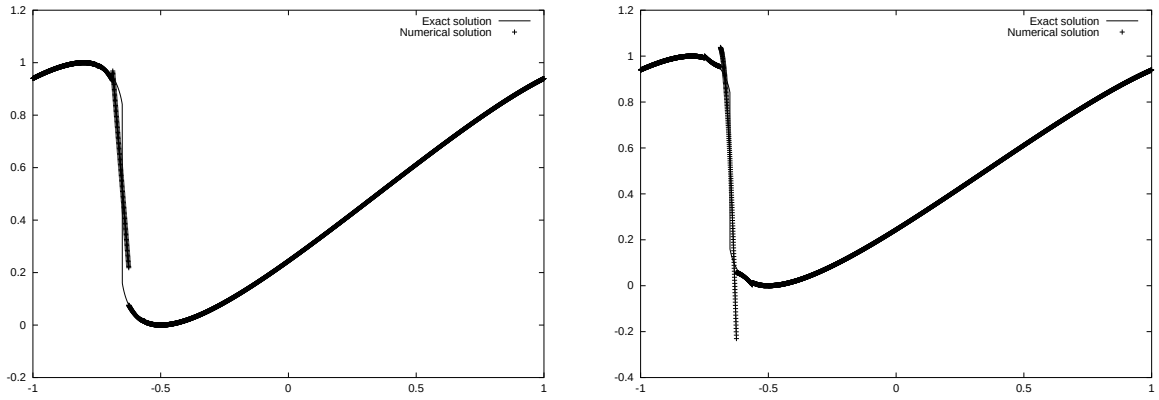

Figure 3: DGM solutions of Example 2 at $t = 0.7$ with $p = 2$ and $N_h = 32$ using moment limiting (left) and no limiting (right) [3]. Computed solutions are shown with $\times$ symbols and exact solutions are shown as solid lines.

Limiting is applied to the highest-order coefficient $c_{p,j}$ in (10a) first. If this coefficient is changed by (13) then limiting is applied to $c_{p-1,j}$. The process continues to limit successively lower-order coefficients until either all coefficients are limited or a coefficient is not changed by (13). Should this occur, Biswas *et al.* [13] assume that no further limiting is necessary. When moment limiting (13) was applied to the kinematic wave equation (12) of Example 1 it produced results with the optimal convergence rate [13]; however, there were counter examples with results having reduced orders of accuracy.

Example 2. We demonstrate the need for limiting with the shock problem for the inviscid Burgers' equation

$$u_t + (\frac{u^2}{2})_x = 0, \qquad t > 0, \qquad u(x,0) = \frac{1 + \sin \pi x}{2}. \tag{14}$$

The solution is periodic on $-1 \leq x < 1$ and the initial sinusoidal data steepens to form a shock which propagates in the positive x direction. DGM solutions with $p = 2$ and $N_h = 32$ are shown at $t = 0.7$ in Figure 3. The solution on the right without limiting exhibits solution overshoots on elements near the shock. These, however, remain localized and the solution is accurate elsewhere. The moment limiting procedure (13) can reduce overshoots without reducing the order of accuracy in smooth solution regions.

3 Error Estimation

Estimates of discretization errors are essential to appraise solution accuracy and are, at the very least, desirable to guide and control adaptive enrichment. *A posteriori* estimates of the discretization errors use the computed solution to gage accuracy and they have been used with adaptive processes since their inception [6]. Ideal *a posteriori* error estimates should be (*i*) inexpensive relative to the cost of the solution; (*ii*) accurate in the sense that they converge to the true error under h- and p-refinement; and (*iii*) robust in the

sense that they provide error bounds over a wide range of mesh spacings, polynomial degrees, and norms. The state of the art regarding error estimation technology is far more advanced for (linear) elliptic and parabolic problems [4, 7, 47] than for transient hyperbolic problems. Nevertheless, some work exists. Süli [42] discusses *a posteriori* estimattion for both linear and nonlinear problems; Houston *et al.* [29, 44] describe procedures for linear problems; Cockburn *et al.* [14, 15] consider nonlinear problems; and Pierce and Giles [36] and Larson and Barth [34] construct *a posteriori* error estimates for linear functional, which can be more important than pointwise error estimates.

Adjerid *et al.* [3] proved that DGM solutions of one-dimensional conservation laws of the form (1) using piecewise-polynomials of degree p on Ω_j have a higher rate of convergence (superconvergence) at the roots of the Radau polynomial of degree $p+1$ than they do elsewhere. The Radau polynomial of degree k is [1]

$$R_k(\xi) = P_k(\xi) \pm P_{k-1}(\xi). \tag{15}$$

The negative sign is chosen when the flow on Ω_j is in the positive coordinate direction (right Radau polynomial) and the positive sign is chosen when the flow is in the negative coordinate direction (left Radau polynomial). With the Legendre polynomials scaled so that $P_k(1) = 1$, $k = 1, 2, \ldots$, and having odd or even symmetry with k, $R_k(\xi)$ will always have a root at the "downwind" end of Ω_j. *Flow* refers to the eigenvalues of $\partial \mathbf{F}_n(\mathbf{u})/\partial \mathbf{u}$; thus, components of the system corresponding to positive eigenvalues will have superconvergence at the roots of right Radau polynomials while those corresponding to negative eigenvalues will vanish near the roots of left Radau polynomials.

A posteriori estimates of discretization errors

$$\mathbf{e}(x,t) := \mathbf{u}(x,t) - \mathbf{U}(x,t) \tag{16}$$

may be obtained using this information by neglecting errors at the roots of $R_{p+1}(\xi)$. In fact, Adjerid *et al.* [3] prove that spatial errors of one-dimensional conservation laws of the form (1) satisfy

$$e_j(x,t) = \alpha_{p+1,j}(t) R_{p+1}(\xi) + O(\Delta x^{p+2}), \qquad \xi \in [-1,1], \qquad x \in \Omega_j, \tag{17a}$$

$$e_j(x_j,t) = O(\Delta x^{2p+1}), \qquad \text{if } \frac{df(u)}{du} > 0. \tag{17b}$$

$$e_j(x_{j-1},t) = O(\Delta x^{2p+1}), \qquad \text{if } \frac{df(u)}{du} < 0. \tag{17c}$$

(The result is stated for a scalar conservation law for simplicity. Results also apply to vector systems [3].) Thus, DGM solutions generally converge as $O(\Delta x^{p+1})$ for $\Delta x = \max(x_j - x_{j-1})$, $j = 1, 2, \ldots, N_h$. Convergence at a slightly faster $O(\Delta x^{p+2})$ rate occurs at the roots of $R_{p+1}(\xi(x))$. However, "ultra fast" $O(\Delta x^{2p+1})$ convergence occurs at the downwind end of each element when $p > 0$. This ultra fast convergence implies that error propagation between elements may be neglected and that error estimates may be obtained by local (element-wise) computations.

The discontinuous Galerkin formulation for a one-dimensional conservation law (1) is

$$\frac{\Delta x_j}{2} \frac{d}{dt} \int_{-1}^{1} \mathbf{v}^T \mathbf{u} d\xi + \mathbf{v}^T \mathbf{F}_n(\mathbf{u})|_{-1}^{1} = \int_{-1}^{1} \mathbf{v}_\xi^T \mathbf{F}(\mathbf{u}) d\xi, \qquad \forall \mathbf{v} \in (\mathcal{L}^2(-1,1))^m. \tag{18a}$$

Finite element solutions are obtained by replacing $\mathbf{u}$ by $\mathbf{U}_j$ according to (10a) and integrating to a given error checking time. The approximate error is obtained by setting

$$\mathbf{u} \approx \mathbf{U}_j + \mathbf{E}_j = \mathbf{U}_j + \boldsymbol{\alpha}_{p+1,j}(t) R_{p+1}(\xi) \tag{18b}$$

in (18a). After testing against polynomials $\mathbf{V} \in (\mathcal{P}^{p+1}(-1,1))^m$, the resulting ordinary differential system is integrated in time for $\boldsymbol{\alpha}_{p+1,j}(t)$. If the ordinary differential equations are integrated to higher order than that used for the DGM solution, we actually obtain an estimate of the global space-time discretization error.

Example 3. We solve the nonlinear wave equation

$$u_{tt} - u_{xx} = u(2u^2 - 1) \tag{19a}$$

which can be written in the form (18a) as

$$(u_1)_t + (u_1)_x = u_2, \qquad (u_2)_t - (u_2)_x = u_1(2u_1^2 - 1) \tag{19b}$$

with $u_1 = u$. We choose the initial and boundary conditions such that the exact solution of (19a) is the solitary wave

$$u(x,t) = \operatorname{sech}(x \cosh \frac{1}{2} + t \sinh \frac{1}{2}). \tag{19c}$$

We solved problems without limiting using polynomials of degrees $p = 0$ to 4. The solution at $t = 1$ performed with $p = 2$ and $N_h = 64$ is shown on the left of Figure 4. Computations illustrating errors and effectivity indices were performed on the more restricted interval $-\pi/3 < x < \pi/3$. Effectivity indices

$$\theta(t) = \frac{\|E_1(\cdot,t)\|_{\mathcal{L}_1}}{\|e_1(\cdot,t)\|_{\mathcal{L}_1}} \tag{20}$$

for the error in $u_1 = u$ with p ranging from 1 to 4 and N_h ranging from 8 to 256 are shown as a function of the degrees of freedom on the right of Figure 4. Effectivity indices are within 0.5% of ideal for all combinations of mesh spacing and $p > 0$. Effectivity indices appear to converge to unity under both h- and p-refinement, for $p > 0$.

3.1 Multi-Dimensional Error Estimation

We may ask whether or not error estimates based on Radau polynomials apply to multi-dimensional problems. Adjerid [2] has shown that (17) applies to two-dimensional problems with tensor-product bases. Herein, we present the nucleus of a theory and some preliminary results for two-dimensional steady, linear problems of the form

$$\vec{a} \cdot \nabla u + cu = r(x,y), \qquad (x,y) \in \Omega, \tag{21}$$

subject to appropriate boundary conditions. Let $\vec{a}$ and c be constants and $r(x,y) \in \mathcal{L}^2(\Omega)$. With this linear flux and an upwind numerical flux, the discontinuous Galerkin formulation (1) of (21) is used with the divergence theorem to obtain

$$\int_{\partial\Omega_j^-} V\vec{a} \cdot \vec{n}(U_j - U^-)d\sigma + \int_{\Omega_j} V(\vec{a} \cdot \nabla U_j + cU_j)d\tau = \int_{\Omega_j} Vr d\tau, \qquad \forall V \in \mathcal{P}^p, \tag{22}$$

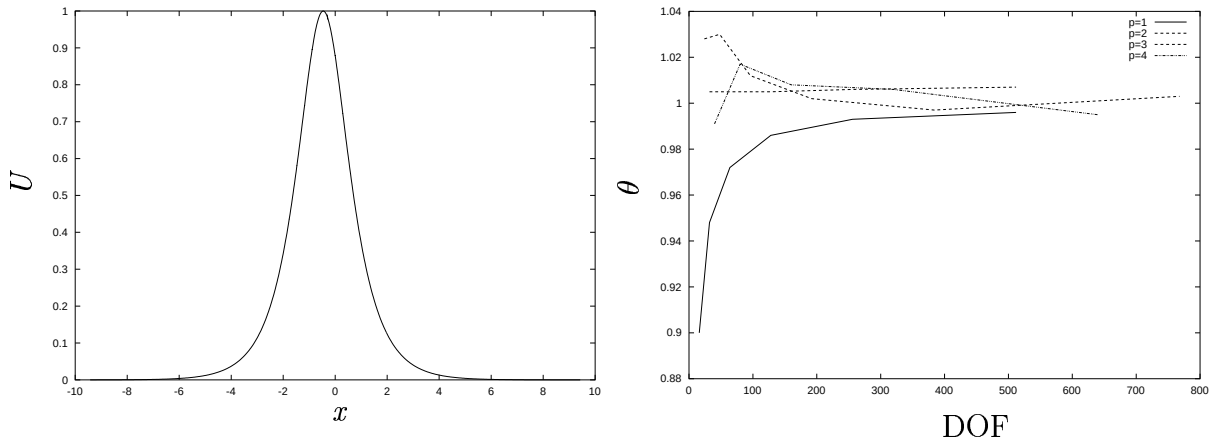

Figure 4: Solution of Example 3 at $t = 1$ on the interval $-3\pi < x < 3\pi$ (left). Global effectivity indices for the solution of (19a) at $t = 1$ as a function of degrees of freedom with p ranging from 1 to 4 (right).

where $\partial\Omega_j^-$ and $\partial\Omega_j^+$ represent the inflow and outflow portions, respectively, of $\partial\Omega_j$. Subtracting the exact solution u from (22) and using the divergence theorem, we obtain the Galerkin orthogonality condition for the local discretization error

$$\int_{\partial\Omega_j^+} \vec{a}\cdot\vec{n}eV\,d\sigma - \int_{\Omega_j} e(\vec{a}\cdot\nabla V - cV)\,d\tau = 0, \qquad \forall V \in \mathcal{P}_p. \tag{23}$$

Mapping Ω_j onto the canonical element Ω_0 (§2.1) yields the scaled equation

$$\int_{\partial\Omega_0^+} \beta eVh\,d\sigma - \int_{\Omega_0} eh(\vec{\alpha}\cdot\nabla V - \gamma Vh)\,d\tau = 0, \qquad \forall V \in \mathcal{P}^p, \tag{24}$$

where $\vec{\alpha}$, β, and γ are constants depending on $\vec{a}$, b, and c and the metrics of the coordinate transformation and h is a mesh-spacing parameter.

Assuming that u is smooth, we expand e in the series

$$e(\xi,\eta) = \sum_{k=0}^{\infty} Q_k(\xi,\eta)h^k \tag{25}$$

and prove that $Q_k \equiv 0$, $0 \le k \le p$. Substituiting (25) into (24) and collecting terms of like powers of h, we further show that the leading (Q_{p+1}) term of (25) satisfies

$$\int_{\Omega_0} Q_{p+1}V\,d\sigma = 0, \qquad \forall V \in \mathcal{P}_{p-1} \tag{26}$$

and

$$\int_{\partial\Omega_0^+} Q_{p+1}V\,d\sigma = 0, \qquad \forall V \in \mathcal{P}_p. \tag{27}$$

h	0.5		0.25		0.125	
p	e	θ	e	θ	e	θ
0	4.85e-02	1.0116	2.49e-04	1.0304	1.49e-02	1.0418
1	8.27e-04	1.0022	2.16e-04	1.0537	7.85e-05	1.0266
2	3.11e-05	0.9609	4.16e-06	0.9267	9.24e-07	0.9054
3	1.71e-06	1.0161	1.04e-07	1.0546	1.47e-08	1.0054
4	1.07e-07	1.0597	3.32e-09	1.0097	2.8e-10	0.9203

Table 1: Computed error and effectivity indices for Example 4.

Using the orthogonal basis (6), we verify that Q_{p+1} has the form

$$Q_{p+1} = \sum_{i=1}^{p+1} c_i^p g_i^p + \sum_{i=1}^{p+2} c_i^{p+1} g_i^{p+1}. \tag{28}$$

(We have added a superscript to g_i in (6) to indicate the polynomial degree. Subscripts indicate the basis elements of a given degree.) With this, we also prove

$$\int_{\partial\Omega_0^+} Q_k \, d\sigma = 0, \qquad k = p+1, p+2 \ldots, 2p+1. \tag{29}$$

This result is analogous to the strong superconvergence at the downwind point in the one-dimensional case. It further implies that error propagation is negligible on the average and it allows us to perform a global error analysis.

As with one-dimensional problems, we construct error estimates by replacing U_j in (22) by $U_j + Q_{p+1,j}(x,y)$ and testing against $V \in \mathcal{P}^{p+1} \backslash \mathcal{P}^p$. This provides $p+2$ equations to determine coefficients c_i^k, $k = p, p+1$. The additional $(p+1)$ equations are obtained by satisfying the exit flow problem (27).

Example 4. We solve the nonlinear problem

$$2u_x + u_y = \frac{3}{2u}, \qquad (x,y) \in (0,1) \times (0,1), \tag{30}$$

with boundary conditions chosen such that the exact solution is

$$u = \sqrt{x+y+1} \tag{31}$$

Computations were performed by integrating a transient problem to steady state. We present error estimates and effectivity indices in Table 1 for computations performed with $p = 0, 1, \ldots, 4$ and $h = 0.125, 0.25, 0.5$. Here h is the longest edge of any triangular element in the mesh. We see that effectivity indices are within 10% of ideal for all combinations of h and p.

4 Adaptivity

We seek enrichment methods where h- and/or p-refinement may be performed on any element at any time. Our procedure uses only local operations to alter element sizes or polynomial degrees and, hopefully, increase, the accuracy and efficiency.

4.1 *p*-Refinement

To increase the degree of an approximation, we initially set the higher-order coefficients in (*e.g.*, (32)) to zero to obtain an identity projection of the existing one. Although a reduction of polynomial degree would seem to be more complex because it may occur either in low-error regions or near discontinuities when limiting is applied. In the former case, the high-order coefficients are small and do not contribute to solution accuracy. However, these coefficients need not be small when limiting is applied. Nevertheless, with an approximation of a function f on Ω_j in the form

$$f = \sum_{i=1}^{N_p} f_i g_i \tag{32}$$

using an orthogonal basis (6), the $\mathcal{L}^2$ projection of $\mathcal{P}^p(\Omega_j)$ onto $\mathcal{P}^q(\Omega_j)$, $q < p$, is obtained by setting the higher-order coefficients f_i, $N_q + 1, N_q + 2, \ldots, N_p$ to zero in (32).

4.2 *h*-Refinement

Modifying element sizes is also straightforward since the DGM does not require interelement continuity. Our current practice [38] is to bisect an element Ω_j into four congruent sub-elements. This quartet may subsequently be coarsened to recover the original element Ω_j. For both refinement and coarsening operations, we determine the new solutions by a $\mathcal{L}^2$ projection. Refinement uses an identity projection. Coarsening will incur a loss of precision.

4.3 Enrichment Strategy

Both h- and p-refinement involve local projections with, mostly, identity operators. Thus, adaptivity with the DGM is fast and accurate. This is important, since dynamic hyperbolic problems will require frequent adaptation over tens of thousands of time steps.

Let the *level of refinement* l_j be the number of h- or p-refinement steps that were necessary to reach the current size or polynomial degree for element j. Also let ϵ_j be an error indicator for element j, which may be one of the discretization error estimates described in §3. If l^{max} is the maximum allowed refinement level and ϵ^{max} is the maximum allowed value of ϵ_j, $j = 1, 2, \ldots, N_h$, then we determine the appropriate refinement level for element j by finding an integer i such that $\epsilon^{max}/d^{i+1} \leq \epsilon_j < \epsilon^{max}/d^i$ and setting $l_j = \max(l^{max} - i, 1)$. The constant d is user prescribed. If, *e.g.*, $d = 10$, then all elements where $\epsilon_j > \epsilon^{max}/10$ will be refined to the maximum level of refinement l^{max}. All elements where $\epsilon^{max}/100 \leq \epsilon_j < \epsilon^{max}/10$ will be refined to level $l^{max} - 1$, *etc.*

4.4 Flow Applications

We demonstrate our adaptive strategy using two classical compressible flow problems involving the Euler equations (2).

Example 5. We consider the reflection of a Mach 10 planar shock by a wedge having a half-angle of 30° [19, 49]. The computational domain (shown with dashed lines in

Figure 5) is a 4×1 unit rectangle oriented along the surface of the wedge. The reflecting wall lies on the bottom of the computational domain, beginning at $x = 1/6$, $y = 0$. Boundary conditions at the top ($y = 1$) are set to those corresponding to the exact motion of a Mach 10 shock. Physical parameters for the gas ahead of the shock are $P_1 = 1$ and $\rho_1 = 1.4$. The Rankine-Hugoniot relations

$$\begin{aligned} v_s = M_s\sqrt{\gamma P_1/\rho_1} = 10, \qquad & P_2/P_1 = (2\gamma M_s^2 - (\gamma - 1))/(\gamma + 1), \\ \rho_2/\rho_1 = (\gamma + 1)M_s^2/((\gamma - 1)M_s^2 + 2), \qquad & \rho_1 v_s = \rho_2(v_s - v_2) \end{aligned} \tag{33}$$

are used to specify post shock conditions.

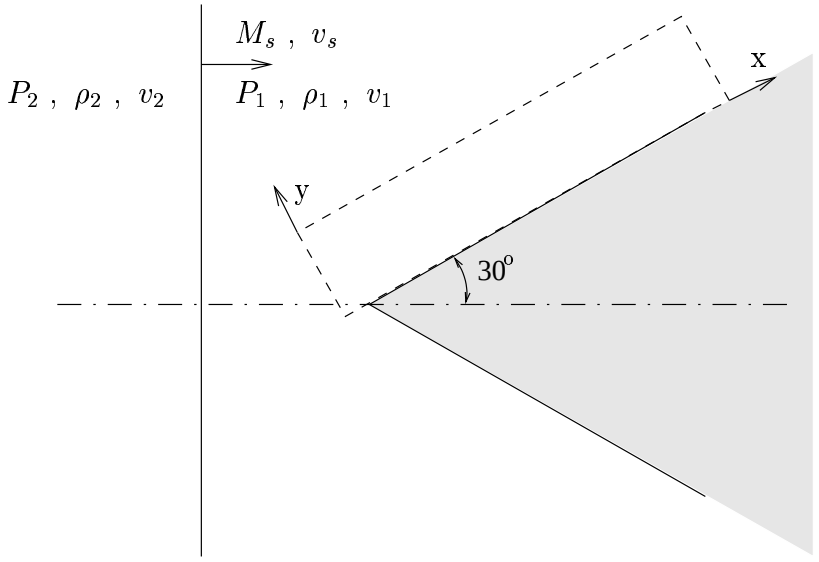

Figure 5: Geometry for the double Mach reflection of Example 5. Conditions ahead of and behind the shock are identified with subscripts 1 and 2, respectively.

Quadrilateral elements are used with tensor products of Legendre polynomials for the spatial discretization [13]. With quadrilaterals, we are able to use moment limiting (§2.3, [13]) to reduce spurious oscillations near shocks and other discontinuities.

Computations were performed with $p = 1$ using $l^{max} = 1$ and 4 and local time stepping [39]. The results at $t = 0.2$ are shown in Figure 6. The shock structure is poorly resolved with only one level of refinement. Discontinuities are diffused over several mesh cells. Results with four refinement levels are much better. Shocks are sharp and the jet formed by the double Mach reflection, usually difficult to capture, is well resolved.

Example 6. Transient computation of unstable flows provide an application where adaptivity in time is crucial. The instability of an interface separating miscible fluids of different densities subject to gravity is known as a *Rayleigh-Taylor Instability* (RTI). Bubbles (spikes) of lighter (heavier) fluid penetrate into the heavier (lighter) fluid, leaving behind a region where the two fluids are mixed. This mixing region quickly becomes irregular and may provide an understanding of turbulence since the flow there has chaotic features [50].

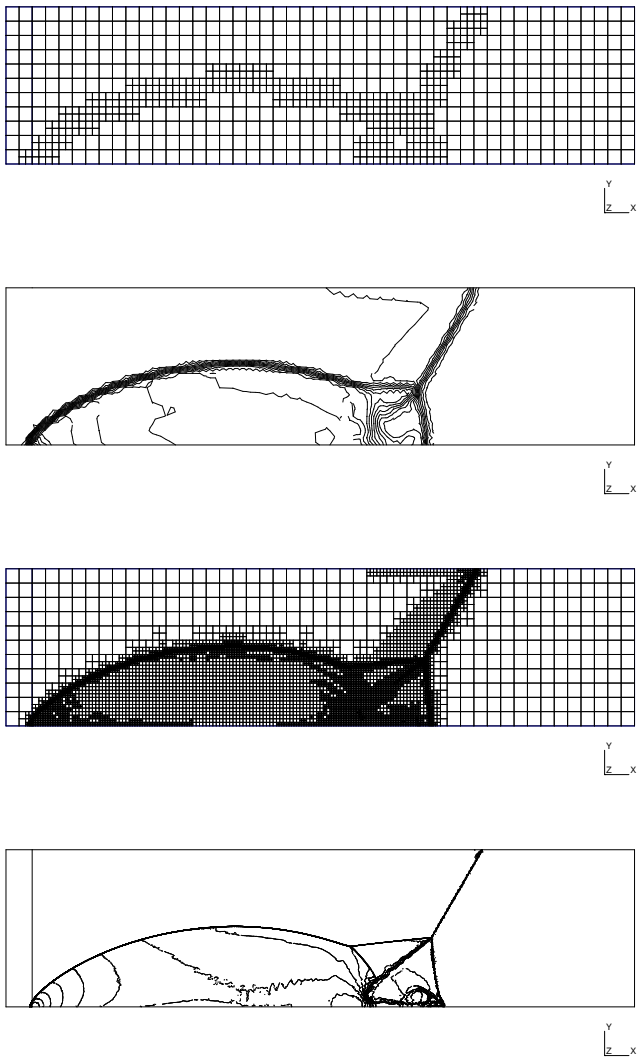

Figure 6: Adaptive grids and density contours for Example 5 at time $t = 0.2$ with $l^{max} = 1$ (top two frames) and $l^{max} = 4$ (bottom two frames).

We address a Rayleigh-Taylor instability in a cavity with a fluid of density $\rho_2 = 2$ above one of density $\rho_1 = 1$ (Figure 7). Neglecting viscosity, fluid motion is governed by the Euler equations (2) with a body force corresponding to (a unit) gravity

$$\mathbf{r} = [0, 0, -\rho, 0]^T . \tag{34}$$

The initial pressure corresponds to (unstable) hydrostatic equilibrium and an initial velocity perturbation initiates the instability. In particular, we perturb the vertical velocity component with 10 Fourier modes having wavelengths $iw/10$, $i = 1, 2, \ldots, 10$, where $w(= 0.25)$ is the width of the cavity.

Without explicit interface tracking [25], adaptive h-refinement will be necessary to accurately represent the complex evolving structure of the bubbles and spikes. We used

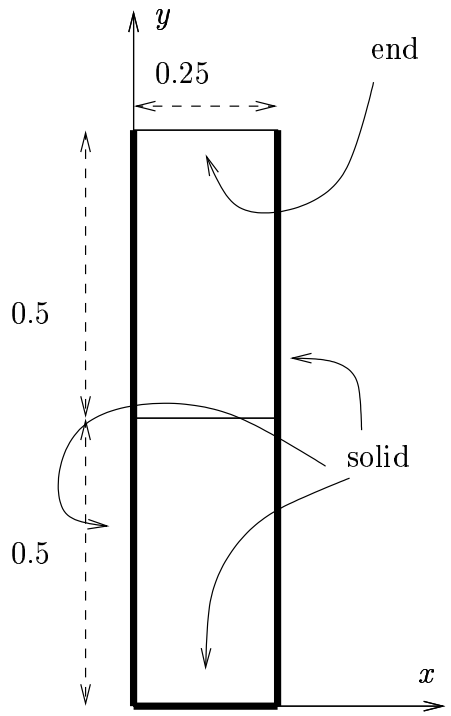

Figure 7: Geometry for the Rayleigh-Taylor instability of Example 6.

the h-refinement procedure described in §4.2 with $l^{max} = 4$. The computation was performed on a four-processor parallel computer with dynamic load balancing used after each refinement step [46].

Figures 8 show the distribution of fluid density and distributed meshes at different times. The refinement is confined to the interface as the complex mixing zone evolves. One basic characteristic of Rayleigh-Taylor instabilities is the constant that describes the acceleration of the mixing zone edge. If

$$A = \frac{\rho_2 - \rho_1}{\rho_2 + \rho_1} \tag{35a}$$

is the Atwood number representing buoyancy due to gravity, the edges of the mixing zone have the asymptotic scaling

$$h = \alpha A g t^2. \tag{35b}$$

Our computation reveals that $\alpha = 0.06$ which agrees with other theoretical and experimental investigations [26].

5 Discussion

We have exposed several properties of the DGM as it applies to hyperbolic conservation laws. We hope that we have demonstrated that the method offers several advantages for flow problems with complex structures. There are still many unresolved issues and

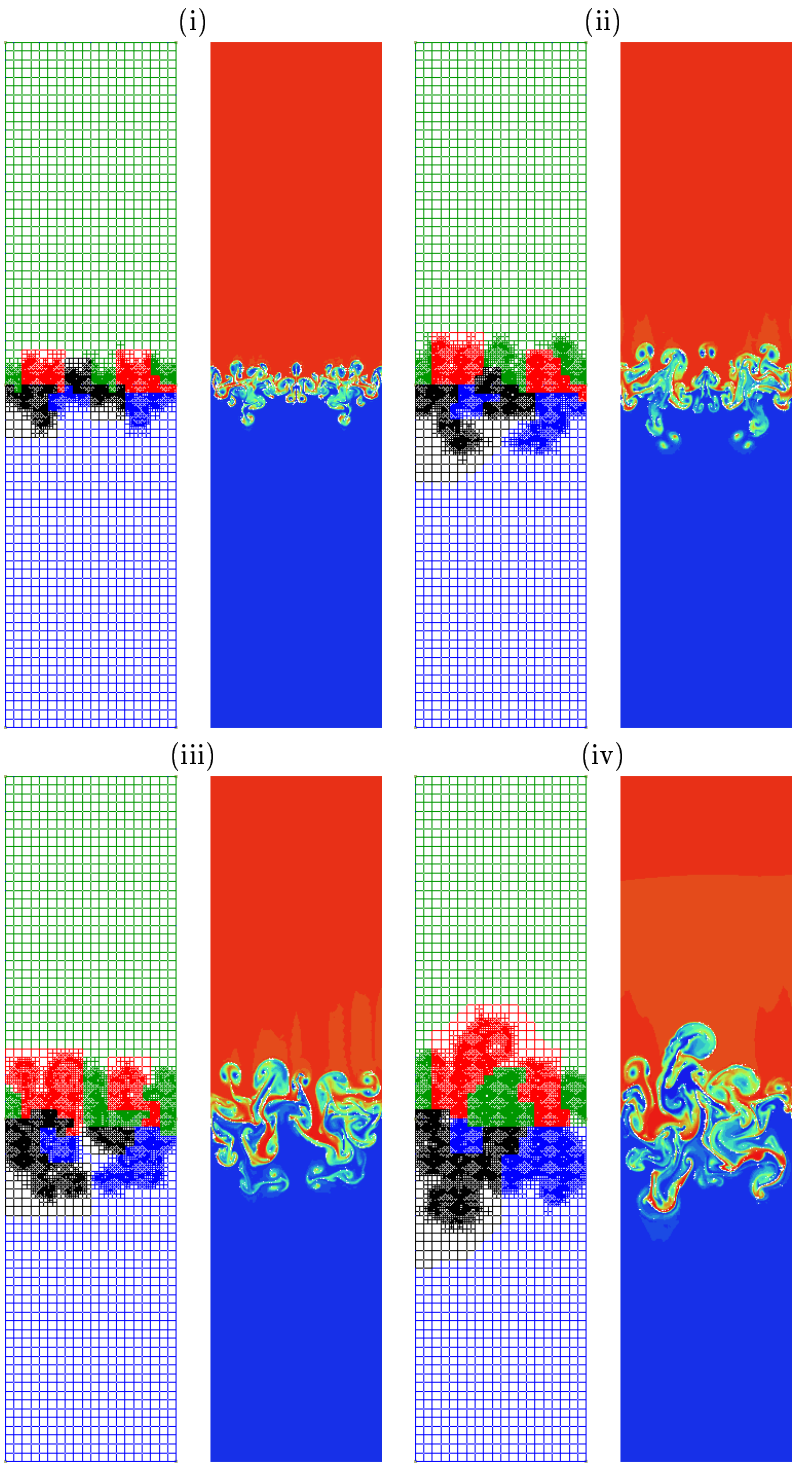

Figure 8: Grids and density contours at $t = 0.5$ (i), $t = 1.0$ (ii), $t = 1.5$ (iii), and $t = 2.0$ (iv) for Example 6 with $l^{max} = 4$. coloring identifies processor assignments on a four-processor parallel computer.

potential improvements to the method. As noted, solution limiting is needed to prevent

spurious oscillations when $p > 0$. This might rely on feature detection such as those that have been used here and elsewhere [13, 18] or it might be based on variation of solution residuals such as procedures used in stabilized finite element methods [30]. Proper use of adaptive *hp*-refinement where low-order ($p = 0$) methods were used at discontinuities and higher-order methods were used in smooth-solution regions could obviate the need for limiting. This would necessitate a discontinuity detection scheme and such strategies may be possible [32, 33].

The error estimation procedures developed here are computationally simple but only apply in smooth solution regions. While they furnish an error indication near discontinuities, more quantitative information is needed.

Of course, there is intense interest in applying the DGM to viscous problems involving, *e.g.*, the Navier-Stokes equations. While procedures exist [9, 8, 48], it is not yet clear as to whether or not they offer computational advantages relative to more traditional finite element or finite difference techniques.

Acknowledgement

Portions of this research were supported by the U.S. Army Research Office (Contract Number DAAG55-98-1-0200), the Department of Energy (Contract Number B341495), the National Science Foundation (Grant Number ASC 9720227), and Sandia National Laboratories (Contract Number AW5657).

References

[1] M. Abramowitz and I.A. Stegun, editors. *Handbook of Mathematical Functions.* Dover, New York, 1965.

[2] S. Adjerid. A posteriori error estimation for hyperbolic partial differential equations. Proceedings of the *Com^{2}MaC Conference on Computational Mathematics*, to appear, 2001.

[3] S. Adjerid, K. Devine, J.E. Flaherty, and L. Krivodonova. A posteriori error estimation for discontinuous Galerkin solutions of hyperbolic problems. *Computer Methods in Applied Mechanics and Engineering*, to appear, 2001.

[4] M. Ainsworth and J.T. Oden. *A posteriori Error Estimation in Finite Element Analysis.* Computational and Applied Mathematics. Elsevier, Amsterdam, 1996.

[5] S. Hou B. Cockburn and C.-W. Shu. The Runge-Kutta local projection discontinuous Galerkin finite element method for the conservation laws IV: The multidimensional case. *Mathematics of Computation*, 54:545–581, 1990.

[6] I. Babuška, J. Chandra, and J.E. Flaherty, editors. *Adaptive Computational Methods for Partial Differential Equations*, Philadelphia, 1983. SIAM.

[7] I. Babuška and T. Strouboulis. *The Finite Element Method and its Reliability.* Oxford University Press, Oxford, 1999. Preliminary edition.

[8] F. Bassi and S. Rebay. A high-order accurate discontinuous finite element method for the numerical solution of the compressible Navier-Stokes equations. *Journal of Computational Physics*, 131:267–279, 1997.

[9] C.E. Baumann and J.T. Oden. A discontinuous hp finite element method for convection-diffusion problems. *Computer Methods in Applied Mechanics and Engineering*, to appear, 2001.

[10] K.S. Bey and J.T. Oden. Hp-version discontinuous Galerkin method for hyperbolic conservation laws. *Computer Methods in Applied Mechanics and Engineering*, 133:259–286, 1996.

[11] K.S. Bey, J.T. Oden, and A. Patra. Hp-version discontinuous Galerkin method for hyperbolic conservation laws: A parallel strategy. *International Journal of Numerical Methods in Engineering*, 38:3889–3908, 1995.

[12] K.S. Bey, J.T. Oden, and A. Patra. A parallel hp-adaptive discontinuous Galerkin method for hyperbolic conservation laws. *Applied Numerical Mathematics*, 20:321–386, 1996.

[13] R. Biswas, K. Devine, and J.E. Flaherty. Parallel adaptive finite element methods for conservation laws. *Applied Numerical Mathematics*, 14:255–284, 1994.

[14] B. Cockburn. A simple introduction to error estimation for nonlinear hyperbolic conservation laws. some ideas, techiques and promising results. In *Proceedings of the 1998 EPSRC Summer School in Numerical Analysis. SSCM, The Graduate Student's Guide to Numerical Analysis*, pages 1–46, Berlin, 1999. Springer Verlag.

[15] B. Cockburn and P.A. Gremaud. Error estimates for finite element methods for nonlinear conservation laws. *SIAM Journal on Numerical Analysis*, 33:522–554, 1996.

[16] B. Cockburn, G. Karniadakis, and C.-W. Shu, editors. *Discontinous Galerkin Methods Theory, Computation and Applications*, volume 11 of *Lecture Notes in Computational Science and Engineering*, Berlin, 2000. Springer.

[17] B. Cockburn, S.Y. Lin, and C.-W. Shu. TVB Runge-Kutta local projection discontinuous Galerkin methods for scalar conservation laws III: One dimensional systems. *Journal of Computational Physics*, 84:90–113, 1989.

[18] B. Cockburn and C.-W. Shu. TVB Runge-Kutta local projection discontinuous Galerkin methods for scalar conservation laws II: General framework. *Mathematics of Computation*, 52:411–435, 1989.

[19] P. Colella and H. M. Glaz. Efficient solution algorithms for the Riemann problem for real gases. *Journal of Computational Physics*, 59:264–289, 1985.

[20] K.D. Devine and J.E. Flaherty. Parallel adaptive hp-refinement techniques for conservation laws. *Applied Numerical Mathematics*, 20:367–386, 1996.

[21] K. Ericksson and C. Johnson. Adaptive finite element methods for parabolic problems I: A linear model problem. *SIAM Journal on Numerical Analysis*, 28:12–23, 1991.

[22] K. Ericksson and C. Johnson. Adaptive finite element methods for parabolic problems II: Optimal error estimates in $l_\infty l_2$ and $l_\infty l_\infty$. *SIAM Journal on Numerical Analysis*, 32:706–740, 1995.

[23] J.E. Flaherty, R. Loy, M.S. Shephard, B.K. Szymanski, J. Teresco, and L. Ziantz. Adaptive local refinement with octree load-balancing for the parallel solution of three-dimensional conservation laws. *Journal of Parallel and Distributed Computing*, 47:139–152, 1997.

[24] J.E. Flaherty, R.M. Loy, M.S. Shephard, and J.D. Teresco. Software for the parallel adaptive solution of conservation laws by discontinuous Galerkin methods. In B. Cockburn, G.E. Karniadakis, and S.-W. Shu, editors, *Discontinous Galerkin Methods Theory, Computation and Applications*, volume 11 of *Lecture Notes in Compuational Science and Engineering*, pages 113–124, Berlin, 2000. Springer.

[25] F. Furtado, J. Glimm, J. Grove, X.-L. Li, W.B. Lindquist, R. Menikoff, D.H. Sharp, and Q. Zhang. Front tracking and the interaction of nonlinear hyperbolic waves. In C.C. Chao, S.A. Orszag, and W. Shyy, editors, *Recent Advances in Computational Fluid Dynamics: Proceedings of the US/ROC (Taiwan) Joint Workshop on Recent Advances in Computational Fluid Dynamics*, volume 43 of *Lecture Notes in Engineering*, pages 99–111, New York, 1989. Springer-Verlag.

[26] J. Glimm, J. Grove, X.L. Li, W. Oh, and D. C. Tan. The dynamics of bubble growth for Rayleigh-Taylor unstable interfaces. *Physics of Fluids*, 31:447–465, 1988.

[27] G.H. Golub and C.F. Van Loan. *Matrix Computations*. The Johns Hopkins University Press, Baltimore, third edition, 1996.

[28] A. Harten and J.M. Hyman. Self-adjusting grid methods for one-dimensional hyperbolic conservation laws. Technical Report LASL Report LA-9105, Los Alamos Scientific Laboratory, Los Alamos, 1983.

[29] P. Houston, E. Süli, and C. Schwab. Stabilized hp-finite element methods for hyperbolic problems. *SIAM Journal on Numerical Analysis*, to appear, 2001.

[30] T. J. R. Hughes, L. P. Franca, and G. M. Hulbert. A new finite element formulation for fluid dynamics: VIII. The Galerkin / least–squares method for advective–diffusive equations. *Computer Methods in Applied Mechanics and Engineering*, 73:173–189, 1989.

[31] C. Johnson. Error estimates and adaptive time-step control for a class of one-step methods for stiff ordinary differential equations. *SIAM Journal on Numerical Analysis*, 25:908–926, 1988.

[32] S. Karni and A. Kurganov. Local error analysis for approximate solutions of hyperbolic conservation laws. Submitted for publication, 2001.

[33] S. Karni, A. Kurganov, and G. Petrova. Soothness indicator for adaptive algorithms. Submitted for publication, 2001.

[34] M. Larson and T. Barth. A posteriori error estimation for discontinuous Galerkin approximations of hyperbolic systems. In B. Cockburn, G. Karniadakis, and C.-W. Shu, editors, *Discontinous Galerkin Methods Theory, Computation and Applications*, volume 11 of *Lecture Notes in Computational Science and Engineering*, pages 363–368, Berlin, 2000. Springer.

[35] B. Van Leer. Flux vector splitting for the Euler equations. Technical Report 82–30, ICASE, NASA Langley Research Center, Hampton, 1982.

[36] N. Pierce and M. Giles. Adjoint recovery of superconvergent functionals from PDE approximation. *SIAM Review*, 42:247–264, 2000.

[37] W.H. Reed and T.R. Hill. Triangular mesh methods for the neutron transport equation. Technical Report LA-UR-73-479, Los Alamos Scientific Laboratory, Los Alamos, 1973.

[38] J.-F. Remacle, J.E. Flaherty, and M.S. Shephard. An adaptive discontinuous Galerkin technique with an orthogonal basis applied to compressible flow problems. *SIAM Review*, submitted, 2000.

[39] J.-F. Remacle, J.E. Flaherty, and M.S. Shephard. An efficient local time stepping scheme for transient adaptive computation. in preparation, 2001.

[40] P.L. Roe. Approximate Riemann solvers, parameter vectors and difference schemes. *Journal of Computational Physics*, 43:357–372, 1981.

[41] P. Le Saint and P. Raviart. On a finite element method for solving the neutron transport equation. In C. de Boor, editor, *Mathematical Aspects of Finite Elements in Partial Differential Equations*, pages 89–145, New York, 1974. Academic Press.

[42] E. Süli. A posteriori error analysis and adaptivity for finite element approximations of hyperbolic problems. In D. Kroner, M. Ohlberger, and C.Rhode, editors, *An Introduction to Recent Developments in Theory and Numerics for Conservation Laws*, volume 5 of *Lecture Notes in Computational Science and Engineering*, pages 123–194, Berlin, 1999. Springer Verlag.

[43] E. Süli and P. Houston. Finite element methods for hyperbolic problems: A posteriori error analysis and adaptivity. In I.S. Duff and G.A. Watson, editors, *The State of the Art in Numerical Analysis*, pages 441–471, Oxford, 1997. Clarendon Press.

[44] E. Süli, C. Schwab, and P. Houston. Hp-DGFEM for partial differential equations with non-negative characteristic form. In B. Cockburn, G. Karniadakis, and C.-W. Shu, editors, *Discontinous Galerkin Methods: Theory, Computation and Applications*, volume 11 of *Lecture Notes in Computational Science and Engineering*, pages 221–230, Berlin, 2000. Springer.

[45] P.K. Sweby. High resolution schemes using flux limiters for hyperbolic conservation laws. *SIAM Journal on Numerical Analysis*, 21:995–1011, 1984.

[46] J.D. Teresco, M.W. Beall, J.E. Flaherty, and M.S. Shephard. A hierarchical partition model for adaptive finite element computation. *Computer Methods in Applied Mechanics and Engineering*, 184:269–285, 2000.

[47] R. Verfürth. *A Review of a Posteriori Error Estimation and Adaptive Mesh-Refinement Techniques*. B.G. Teubner, Stuttgart, 1996.

[48] M.F. Wheeler. An elliptic collocation-finite element method with interior penalties. *SIAM Journal on Numerical Analysis*, 15:152–161, 1978.

[49] P. Woodward and P. Colella. The numerical simulation of two-dimensional fluid flow with strong shocks. *Journal of Computational Physics*, 54:115–173, 1984.

[50] Y.-N. Young, H. Tufo, A. Dubey, and R. Rosner. On the miscible Rayleigh-Taylor instability. J. Fluid Mech., submitted, 2000.